

Supplementary Information for

Cobalt-to-vanadium charge transfer in

polyoxometalate water oxidation catalysts revealed

by 2p3d resonant inelastic x-ray scattering

*Boyang Liu,[†] Elliot N. Glass,[§] Ru-pan Wang,[†] Yi-tao Cui,[‡] Yoshihisa Harada,[‡] Di-jing Huang,^{||}
Stefan Schuppler,[⊥] Craig L. Hill,[§] and Frank F.M. de Groot^{*,†}*

[†] Inorganic Chemistry & Catalysis, Debye Institute for Nanomaterials Science, Utrecht University, Universiteitsweg 99, 3584 CG, The Netherlands

[§] Department of Chemistry, Emory University, Atlanta, Georgia 30322, United States

[‡] Institute for Solid State Physics, The University of Tokyo, Kashiwa, Chiba 277-8581, Japan

^{||} National Synchrotron Radiation Research Center, Hsinchu 30076, Taiwan

[⊥] Institut fuer Festkorperphysik, Karlsruhe Institute of Technology, Karlsruhe 76021, Germany

UV-vis and FT-IR data of Co_4P_2 and Co_4V_2

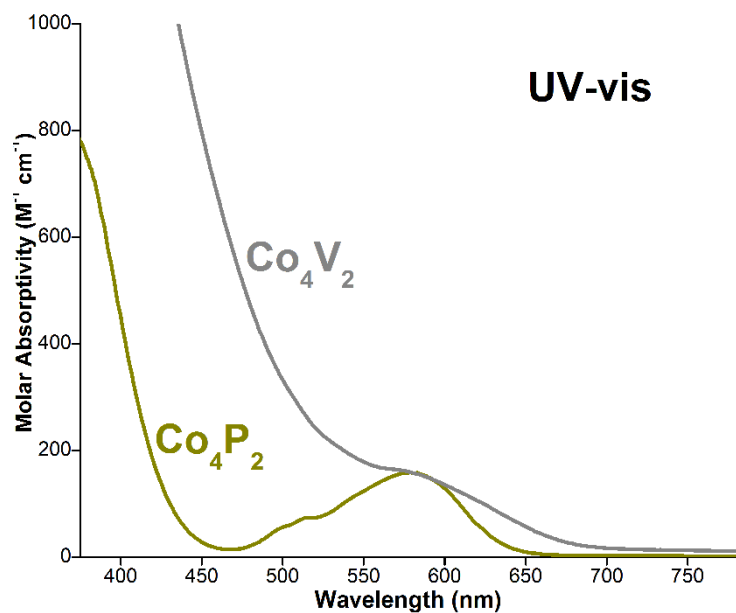


Figure S1. UV-vis spectra of Co_4P_2 and Co_4V_2 .

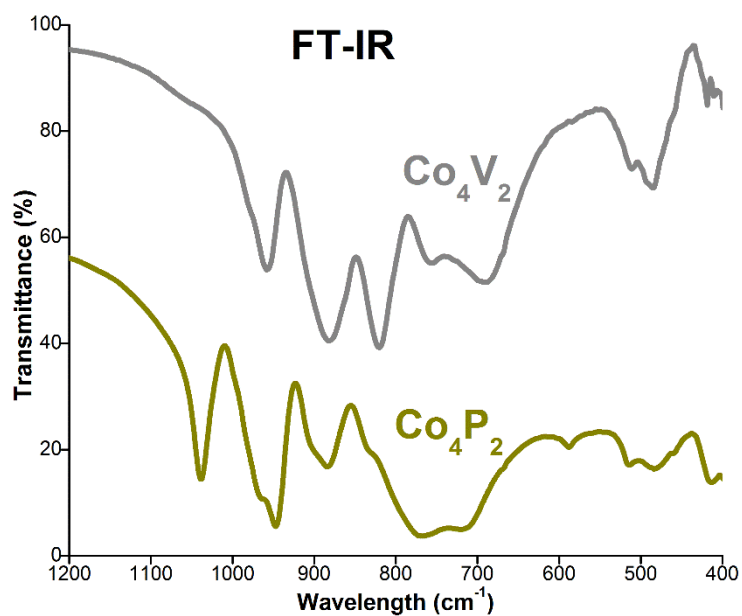


Figure S2. FT-IR spectra of Co_4P_2 and Co_4V_2 .

Theoretical basis

LFM calculations were performed to simulate the cobalt XAS and RIXS spectra. The LFM codes used in this work are the Cowan-Butler-Thole's code,¹⁻³ which allows the description of transitions in XAS and RIXS spectra using atomic multiplet, ligand field and superexchange fields. Since cobalt centers in both POM samples are in the 2+ oxidation state,^{4, 5} effects of ligand charge transfer are ignored, resulting in single $2p^63d^7$, $2p^53d^8$ and $2p^63d^8\bar{d}$ electron configuration descriptions of initial, intermediate (final for XAS) and final states of the RIXS process, respectively. Here, the $3d^8\bar{d}$ notation is used rather than the $3d^7$ notation to represent possible d-d transitions. Also, in contrast to the X-ray photoemission spectroscopy (XPS), both XAS and RIXS processes are *charge-neutral*, so minor charge transfer effects need to be considered. Moreover, because d-d transitions are the dominant features in cobalt 2p3d RIXS spectra, the role of vanadium 3d orbitals are neglected in simulations of cobalt spectra. We note that the LFM calculation contains a number of empirical parameters that can effectively describe the electron-electron (2p3d and 3d3d) interactions, spin-orbit couplings and the ligand field splittings.⁶⁻⁹ Such an approach captures the essence of XAS and RIXS processes, which is capable of providing relatively precise insights into the 3d-orbital rich states. The RIXS simulations are based on the Kramers-Heisenberg equation,^{6, 10} and the interference effects between the core excited process and the radiative decay process in RIXS are taken into account. The LH polarization is calculated using the summation of $[\sigma_{in} \text{ to } \pi_{out}]$ and $[\pi_{in} \text{ to } \sigma_{out}]$ polarizations. The simulated transitions are convoluted with a Lorentzian and a Gaussian function to account for the lifetime and the instrumental-induced broadenings respectively. In the simulation of TEY XAS spectra, Boltzmann weighted states are included to account for the room temperature populated states. The PFY XAS spectra are simulated by integrating the 2p3d RIXS plane along the incident energy, since the 2p3d X-ray emission channel is the dominant radiative channel and other weaker channels such as 2p3s and 2p4s are ignored.

Table S1. Electronic structure parameter values used in LFM simulations of 2p XAS and 2p3d RIXS spectra of **Co₄V₂** and **Co₄P₂**. Parameter values of the RIXS final state are equivalent to the corresponding initial state and are not shown.

Parameters (eV)	Initial state Co₄V₂ / Co₄P₂	Final state (XAS) & Intermediate state (RIXS) Co₄V₂ / Co₄P₂
F_{dd}^2	10.005 / 10.145	10.716 / 10.856
F_{dd}^4	6.709 / 7.397	7.208 / 7.908
F_{pd}^2		7.260 / 7.260
G_{pd}^I		4.857 / 4.857
G_{pd}^3		3.069 / 3.069
$\mathbf{L} \cdot \mathbf{S}_d$	0.066 / 0.066	0.083 / 0.083
$\mathbf{L} \cdot \mathbf{S}_p$		9.748 / 9.748
10Dq	0.870 / 0.930	0.870 / 0.930
Ds	0.040 / 0.050	0.040 / 0.050
Dt	-0.005 / 0.000	-0.005 / 0.000
M	0.0003 / 0.0003	0.0003 / 0.0003
<hr/>		
Parameters (atomic value %)		
F_{dd}^2	86 / 88	86 / 88
F_{dd}^4	93 / 102	93 / 102
F_{pd}^2		100 / 100
G_{pd}^I		90 / 90
G_{pd}^3		100 / 100
$\mathbf{L} \cdot \mathbf{S}_d$	100 / 100	100 / 100
$\mathbf{L} \cdot \mathbf{S}_p$		100 / 100

Comparisons of vanadium 2p XAS acquired in ANKA and SPring-8

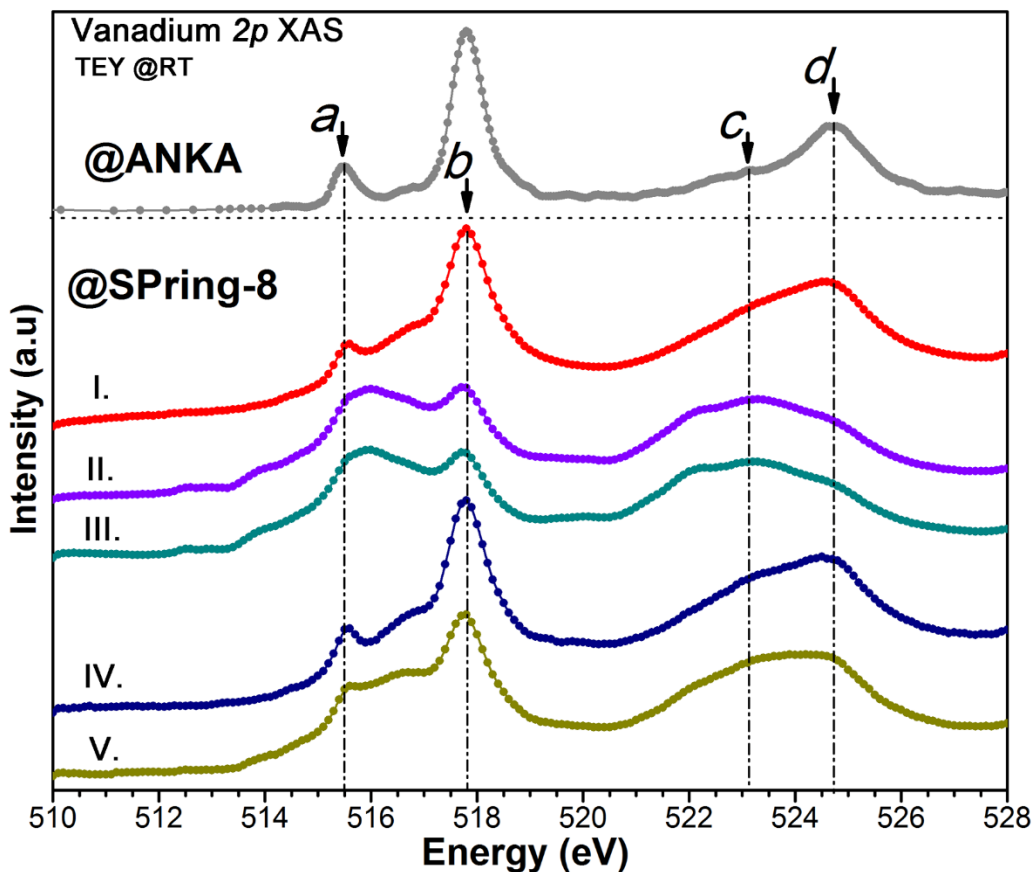


Figure S3. Vanadium experimental 2p XAS: (upper panel) data acquired at the WERA beamline in ANKA synchrotron; (lower panel) data acquired at HORNET endstation, BL07LSU in the SPring-8 synchrotron. Arrows *a-d* indicate the excitation energies of 2p3d RIXS. The spectra I-V acquired at SPring-8 were measured at: (I) a new pristine position; (II) the same position as I; (III) the same position as I and II; (IV) a new pristine position; (V) the same position as IV on the pressed sample pellet.

In Figure S3, the vanadium 2p XAS acquired from ANKA (upper panel) and SPring-8 (lower panel) are compared. The spectra from SPring-8 shows the beam induced photoreduction of vanadium 5+ ions. The two spectra (I and IV) that were measured at a pristine new sample position show higher intensity at peak *c*. For spectra II, III, acquired at the same sample position as spectrum I, and spectrum V, acquired at the same sample position as spectrum IV, the intensity of peak *c* is increased. This change in intensity is consistent with the photoreduction of vanadium 5+ to 4+. ⁵⁹ The 1.5 eV difference of peak *c* and *d* is approximately the L₂ edge maxima between

vanadium 4+ and 5+, suggesting that the RIXS spectrum acquired with excitation energy c , if the photoreduction effect is unavoidable within the fast scan mode of RIXS measurement, shows the most prominent vanadium 4+ RIXS d-d features.

X-ray crystallographic results of Co_4P_2 and Co_4V_2

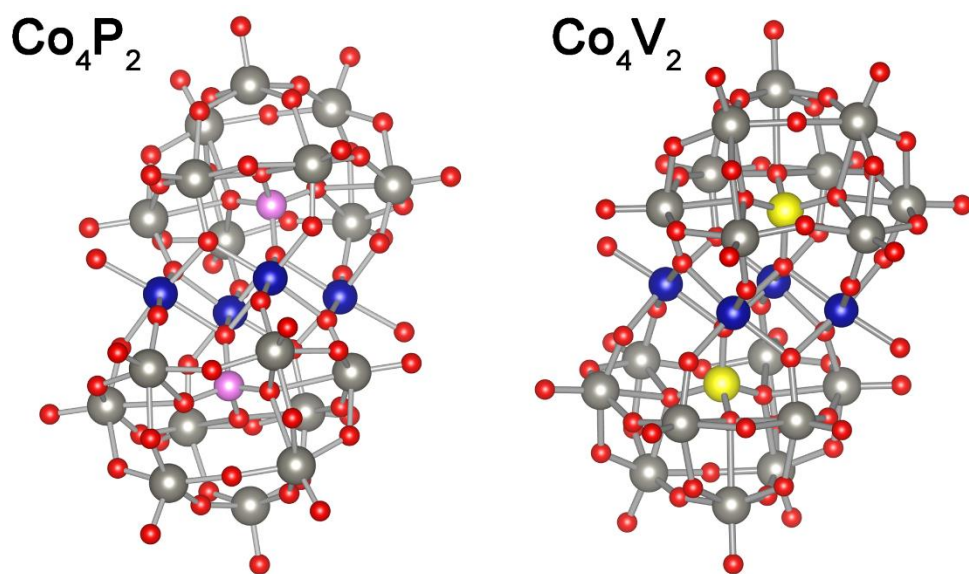


Figure S4. X-ray crystal structures of Co_4P_2 and Co_4V_2 in ball-and stick representations.

Experimental cobalt 2p XAS of Co_4P_2 and Co_4V_2 acquired in ANKA with TEY (at room temperature) and PFY (at 50K) mode respectively

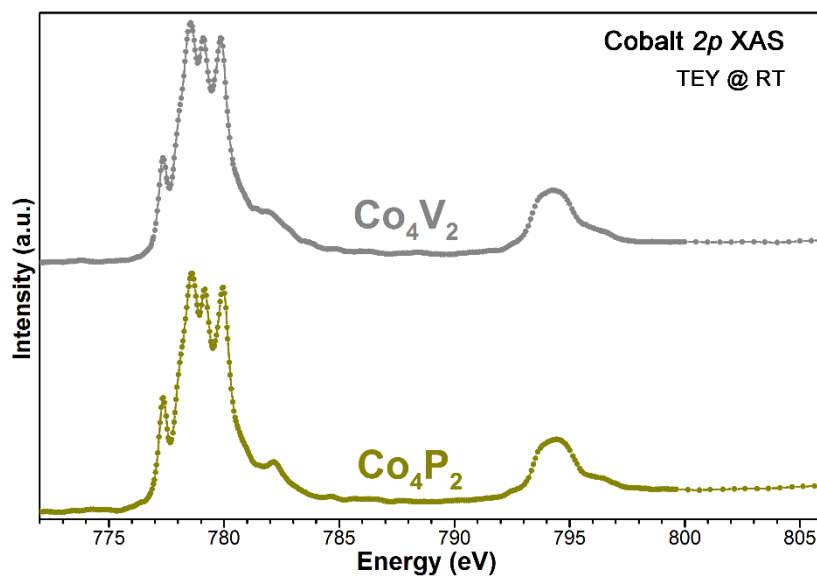


Figure S5. Experimental cobalt 2p XAS spectra of Co_4P_2 (lower, dark yellow) and Co_4V_2 (upper, gray) acquired at the ANKA synchrotron, with TEY mode at room temperature.

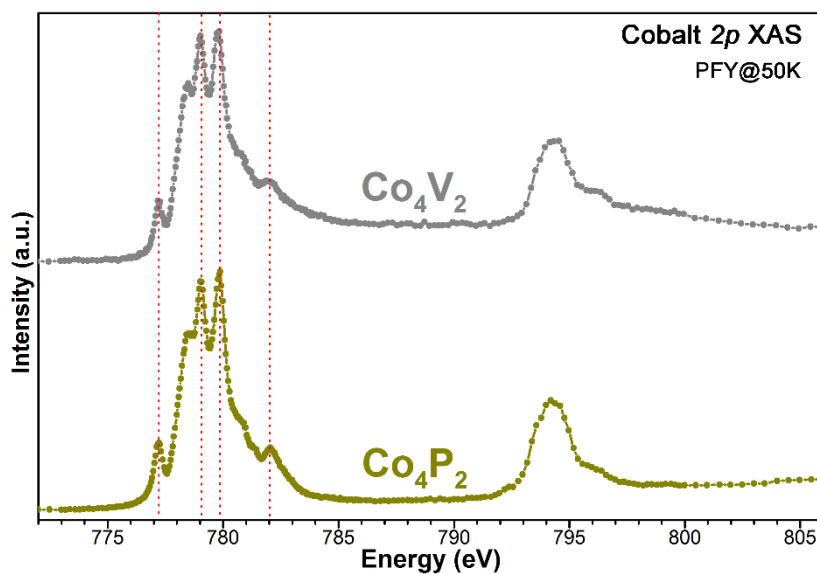


Figure S6. Experimental cobalt 2p XAS spectra of Co_4P_2 (lower, dark yellow) and Co_4V_2 (upper, gray) acquired at the ANKA synchrotron, with PFY mode at 50 K.

Comparison of experimental cobalt 2p XAS and 2p3d RIXS spectra of Co_4P_4 , Co_4P_2 and Co_4V_2

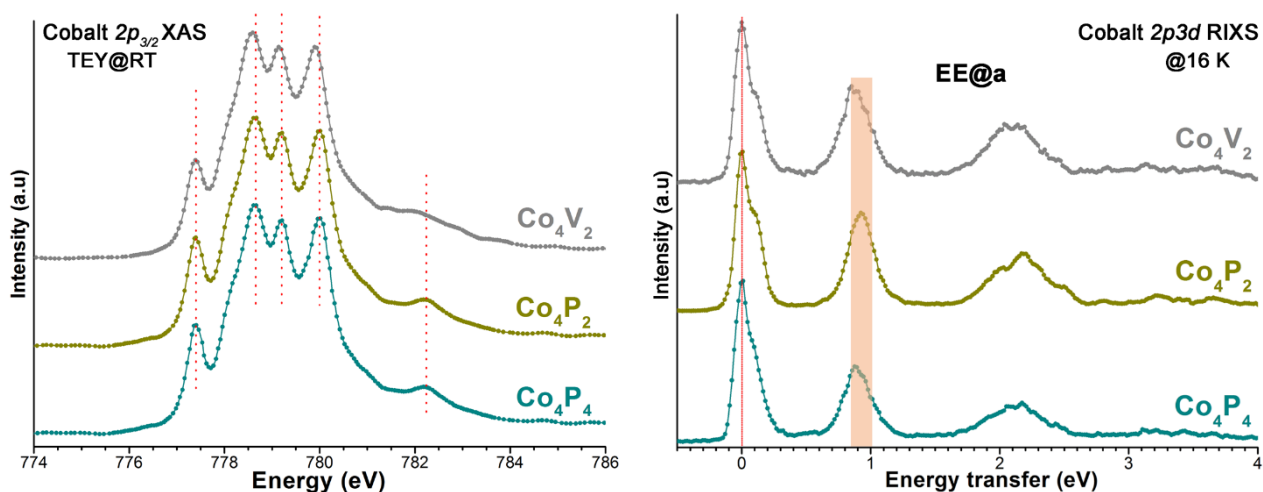


Figure S7. Experimental cobalt $2p_{3/2}$ TEY XAS (left panel) and $2p3d$ RIXS (right panel) spectra of **Co_4P_4** (bottom, green), **Co_4P_2** (middle, dark yellow) and **Co_4V_2** (top, gray). **Co_4P_4** represents $\text{Na}_{16}[\text{Co}_4(\text{H}_2\text{O})_2(\text{P}_2\text{W}_{15}\text{O}_{56})_2] \cdot x\text{H}_2\text{O}$,¹¹ which has the same isostructural tetra-cobalt core as **Co_4P_2** and **Co_4V_2** . RIXS spectra were acquired with the excitation energy a , indicated in Figure 2.

In $2p_{3/2}$ XAS of **Co_4P_2** and **Co_4P_4** , the red-dotted lines indicate the same positions of all prominent multiplet peaks, from which the same LFM parameters may be used for simulating spectra. In contrast to $2p3d$ RIXS, the first d-d excitation peak of **Co_4P_2** and **Co_4P_4** shows observable deviations that indicate a smaller (effective) ligand field strength of the tetra-cobalt core in **Co_4P_4** . This example implies that differences shown in the $2p_{3/2}$ XAS of **Co_4P_2** and **Co_4V_2** may not be enough to demonstrate detailed ligand field information, while $2p3d$ RIXS results are more sensitive, resulting in higher accuracy. Fortunately, for **Co_4P_2** and **Co_4V_2** , $2p$ XAS and $2p3d$ RIXS results can be interpreted with a unique set of LFM parameters (in Table S1), suggesting the effectiveness of the LFM parameters found.

Gaussian fit of ~0.9 eV d-d excitation peaks of cobalt RIXS spectra

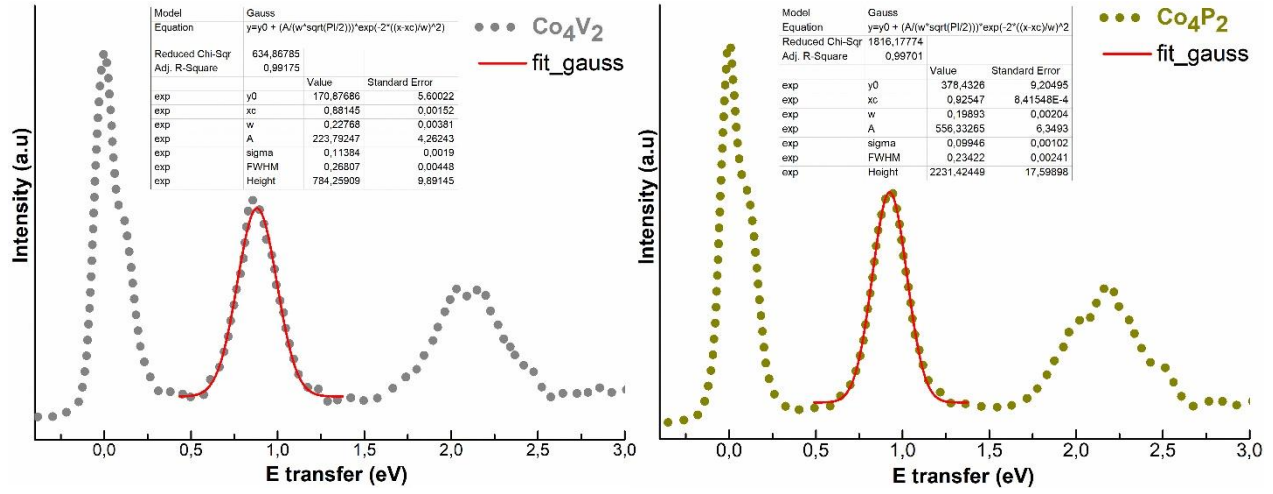


Figure S8. Gaussian peak fit of the ~0.9 eV d-d excitation in cobalt RIXS spectra of (left) Co_4V_2 and (right) Co_4P_2 .

Gaussian fit results indicate that the first d-d peak positions are 925 meV and 881 meV respectively for Co_4V_2 and Co_4P_2 , with uncertainties less than 1 meV for both fits. These fitted results form the basis for the 10Dq parameter in the spectral simulations.

LFM simulated cobalt 2p3d RIXS planes of Co_4V_2 and Co_4P_2

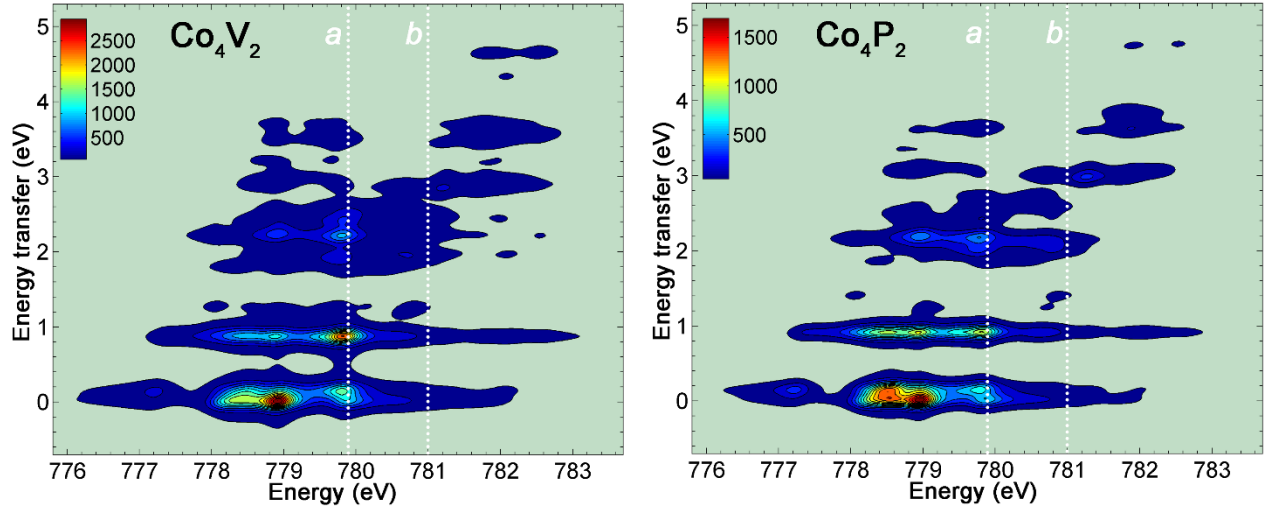


Figure S9. LFM simulated cobalt 2p3d RIXS planes of Co_4V_2 (left) and Co_4P_2 (right). The white dotted lines *a* and *b* in both RIXS planes correspond to the excitation energies *a* and *b* indicated in Figure 2.

LFM simulated 2p3d RIXS plane of the vanadium 4+ ion

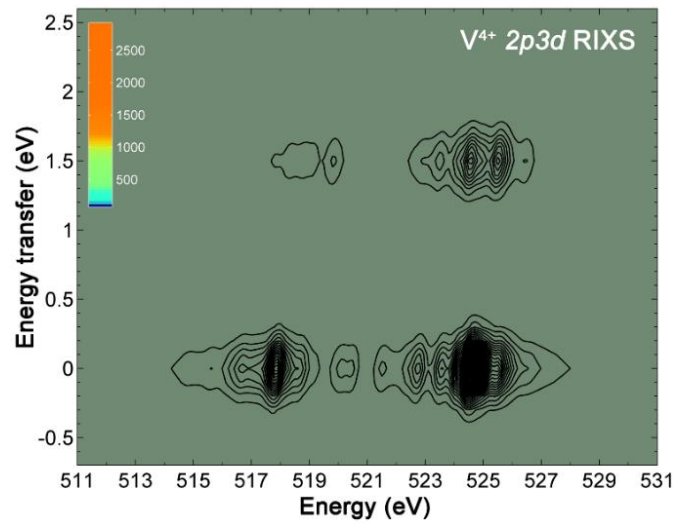


Figure S10. LFM simulated 2p3d RIXS plane of the vanadium 4+ ion, with the ligand field strength $10Dq$ of -1.5 eV.

References

1. R. D. Cowan, *J. Opt. Soc. Am.*, 1968, **58**, 808-818.
2. R. D. Cowan, *University of California Press, Berkeley, CA*, 1981.
3. B. T. Thole, G. van der Laan and P. H. Butler, *Chem. Phys. Lett.*, 1988, **149**, 295-299.
4. Q. S. Yin, J. M. Tan, C. Besson, Y. V. Geletii, D. G. Musaev, A. E. Kuznetsov, Z. Luo, K. I. Hardcastle and C. L. Hill, *Science*, 2010, **328**, 342-345.
5. H. J. Lv, J. Song, Y. V. Geletii, J. W. Vickers, J. M. Sumliner, D. G. Musaev, P. Kogerler, P. F. Zhuk, J. Bacsá, G. B. Zhu and C. L. Hill, *J. Am. Chem. Soc.*, 2014, **136**, 9268-9271.
6. de Groot F.M.F and Kotani. A, *CRC Press* 2008.
7. M. M. van Schooneveld, R. W. Gosselink, T. M. Eggenhuisen, M. Al Samarai, C. MonnTEY, K. J. J. Zhou, T. Schmitt and F. M. F. de Groot, *Angew. Chem. Int. Edit.*, 2013, **52**, 1170-1174.
8. B. Y. Liu, R. P. Wang, E. N. Glass, C. L. Hill, T. Cuk, J. Okamoto, D. J. Huang, M. M. van Schooneveld and F. M. F. de Groot, *Inorg. Chem.*, 2016, **55**, 10152-10160.
9. F. M. F. de Groot, J. C. Fuggle, B. T. Thole and G. A. Sawatzky, *Phys. Rev. B*, 1990, **41**, 928-937.
10. H. A. Kramers and W. Heisenberg, *Z. Phys*, 1925, **1**, 681-701.
11. R. G. Finke, M. W. Droege and P. J. Domaille, *Inorg. Chem.*, 1987, **26**, 3886-3896.